Resolving Complex Shape Distortions on Narrow, Thin Gauge Strip Having an Asymmetric Transverse Thickness Profile — Case Study: Part 2 — Resolving the Problem

Resolving localized shape distortions in narrow, asymmetric profiled strip is a difficult, multi-faceted problem. There are many potentially coupled and interacting sources, and no easy way to find the culprit. A recently developed analytic method offers a means of decoupling and isolating the individual components, providing insight into the fundamental problem and avenues of correction. This article is the second in a two-part case study and provides an illustration of how the analytic method can be applied.

This article is the sixth in a series by Mark E. Zipf. The preceding parts were published in sequence in the December 2012, February 2013, February 2014, December 2014 and May 2016 issues of *Iron & Steel Technology*.

Author

Mark E. Zipf
control, automation and drive systems, Cold Rolling Technologies Inc., Middlefield, Conn., USA
mzipf@istcrt.com

Part 1 of this case study[1] provided an overview of the process, the material, the mill, and the shape distortion, and defined the problem at hand. Historically, the strategies employed in resolving these types of problems range from trial and error to the insight of experience (i.e., little black notebooks and tribal knowledge). As pointed out in previous articles,[3,5] there are often several viable paths to resolution, which only adds confusion and uncertainty on how best to proceed.

This article completes this case study by employing a recently developed method[2–5] to expose and examine the details of the underlying problem. As shown in Fig. 1, the approach taken here analytically decomposes (to characterize and understand) the mill/material interactions into the fundamental components involved in forming the rolled/exit strip shape, and examines their influences, sensitivities, couplings and interactions with respect to the nature of the defect.

Through empirical/direct measurement, parameter identification studies, and knowledge of the mill's mechanics and setup/operating practices, the nature of these components can be determined. These determinations configure and calibrate the analytic model, while also exposing any idiosyncrasies (distortions, behavior, etc.) unique to the mill, material, setup and operations in question.

Correlating the analytic descriptions of the mill with the characteristics of the problematic shape distortion provides a means of examining how the shape defect is formed and transmitted to the rolled/exit strip.

Knowing and understanding the formation/transmission relationship provides immediate insight into the available pathways of resolution. Using analytic simulation, it is possible to test and evaluate the various solution scenarios (trial runs in advance of taking any actions) to help determine the best course of action.

Figure 1

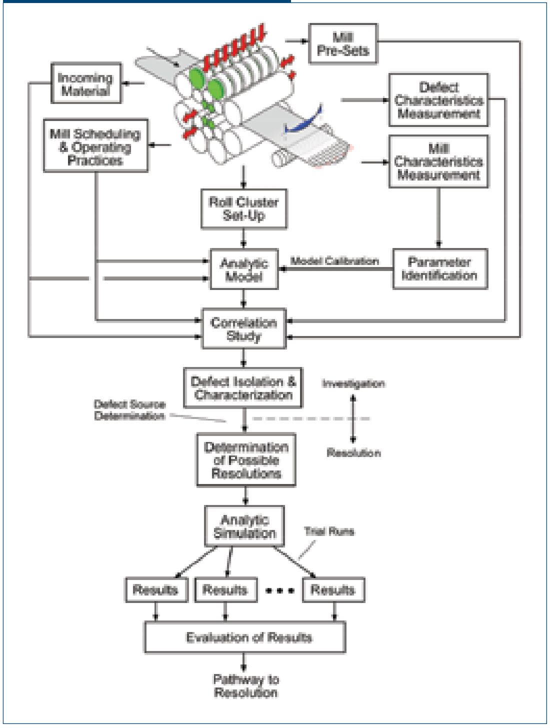

Procedural flow of the analytic method.

Understanding the Involved Components

In addressing this problem, it is important to keep in mind that while one may be confronted with riddles and mysteries, there is no "magic" going on in the mill or material. This is a complex mechanics problem with many potential, interacting sources, and Sir Isaac Newton is the "master of ceremony" at this show. So, one must keep an open mind and start by identifying/characterizing the potential sources, and methodically peel back the layers of the situation.

An analytic method[2–5] will be employed that offers a means of decoupling and isolating the individual components, thus providing insight into the source of the problem and avenues of correction. As discussed in Part 1 of this case study, central to this approach is the transverse superposition of contributing factors, provided by the vector summation of the spatial waveforms:[2]

$$\mathbf{S}_T(y_M) \sim \mathbf{S}(y_M) = \mathbf{S}_0(y_M) + \mathbf{S}_R(y_M) + \mathbf{S}_A(y_M)$$

(Eq. 1a)

$$\mathbf{S}_T(y_M) \sim \mathbf{S}(y_M) = \mathbf{S}_0(y_M) + \mathbf{S}_R(y_M) + \mathbf{G}_M\mathbf{A}$$

(Eq. 1b)

where these shape/stress components are the discrete, spatial representations (across the strip width at normalized, bipolar locations y_M)[2] of the contributing transverse shape/stress waveform patterns. These are physical entities that can be modeled and, in many cases, directly measured.

These complex spatial waveform patterns are composed of weighted, lower-order curvatures formed by Gram orthogonal polynomials.[2] The collection of weighted order curvatures forms a distribution or spectrum that is unique to the individual waveform. The normalized, orthogonal polynomial basis provides a bi-directional transformation that is purely matrix algebraic (i.e., the inverse of the transformation matrix is its transpose).

$$\mathbf{S} = \tilde{\mathbf{P}}\$_S \qquad \$_S = \tilde{\mathbf{P}}^T\mathrm{S}$$

(Eq. 2)

where $\tilde{\mathbf{P}}$ is the normalized, curvature parameter decomposition transform matrix.[2] This is a highly convenient mathematical arrangement. The corresponding curvature representations (spectra) are given by:

$$\$_T \sim \$_S = \$_0 + \$_R + \$_A$$

(Eq. 3a)

$$\$_T \sim \$_S = \$_0 + \$_R + \tilde{\mathbf{P}}^T\mathbf{G}_M\mathbf{A}$$

(Eq. 3b)

where

$\mathbf{S}(y_M) \Leftrightarrow \$_S$	$\triangleq$	Rolled/existing strip shape pattern and associated spatial curvature spectrum,
$\mathbf{S}_T(y_M) \Leftrightarrow \$_T$	$\triangleq$	Shape target pattern and associated spatial curvature spectrum,
$\mathbf{S}_0(y_M) \Leftrightarrow \$_0$	$\triangleq$	Incoming strip shape pattern and associated spatial curvature spectrum,
$\mathbf{S}_R(y_M) \Leftrightarrow \$_R$	$\triangleq$	Mill's mechanical deformation shape pattern and associated spatial curvature spectrum,
$\mathbf{S}_A(y_M) \Leftrightarrow \$_A$	$\triangleq$	Shape actuation–induced shape pattern and associated spatial curvature spectrum,
$\mathbf{G}_M$	$\triangleq$	Mill's shape actuation characterization/transmission matrix and
$\mathbf{A}$	$\triangleq$	Mill's shape actuator setting.

The extent of curvatures in the rolled/exit shape (stress) reachable by the constrained/limited shape actuation settings is defined by the closed region of the *Offset* SACE (shape actuation capabilities envelope),[2] and is where the given pass' operating point may lie.

$$\$_T \sim \$_S \subseteq \$_0 + \$_R + \{\$_{\bar{A}}\} = \$_0 + \$_R + \tilde{\mathbf{P}}^T\mathbf{G}_M\bar{\mathbf{A}}$$

(Eq. 4)

where

$\{\$_{\bar{A}}\}$	$\triangleq$	SACE: The closed set of shape adjustment curvatures associated with all possible shape actuation settings constrained by the imposed operational and physical limits and
$\bar{\mathrm{A}}$	$\triangleq$	Set of constrained/limited shape actuation settings.

Expanding on the Contributors — The focus is a reversing, multi-pass reduction process and the pass-to-pass shape progression[3,5] will be controlled in a closed-loop sense; therefore, a degree of flexibility is granted by adjusting the shape targeting, $\mathbf{S}_T(y_M)$, and subsequently the incoming shape, $\mathbf{S}_0(y_M)$, in the later passes. Realistically, the complex behavior of the wedged strip and its complex coiling behavior will need to be dealt with, which will introduce a characteristic disturbance in the applied transverse tension profile, possibly leading to confusion and unexpected results. In this case, the $\mathbf{S}_0(y_M)$ term can be augmented with a component representing the disturbing effects of the strip profile and coiling influence, $\mathbf{S}_0^{Dist}(y_M)$, which may/will vary with the coil buildup.

The shape actuation component, $\mathbf{S}_A(y_M)$, is dynamic and can be adjusted during rolling operations. The physical/spatial waveform patterns of the shape actuators are well-defined[2] and can be found by direct testing.[6] One important aspect of the shape actuation is the pre-set pattern applied (to the top crown eccentrics (TCEs) and the positioning of the first intermediate rolls (first IMRs)), as an initial condition (an additional offset from the nominal operating point to a point within the *Offset* SACE), prior to rolling a pass. The pre-setting of the TCEs is primarily a method to induce or reduce the cluster's total effective crown (superposition of both the mechanical (ground-in) roll diameter profile and the assistance of the TCEs' pre-set pattern). Any non-zero pre-setting of the shape actuation system will have an impact on the constrained control range (i.e., the extent of the available shape adjustments),[2,3,5] leaving a reduced dynamic range for applying shape corrections. Due to their static nature, this offsetting factor of the pre-sets can be associated with the mill's mechanical deformation.

The mill's mechanical deformation term, $\mathbf{S}_R(y_M)$, is a composite formed from the interactions of the material geometry and yield stress, applied separating force, the force loaded roll cluster deflection, the setup of the roll profiles and tapers, the roll cluster flexibility,[3,6] mill housing, etc. It also carries with it the possibly odd or curious idiosyncrasies unique to the mill in question. This component is static and cannot be modified during on-line/rolling operations.

$$\mathbf{S}_R = \mathbf{S}_R^{NL} + \mathbf{S}_R^{FSep} + \mathbf{S}_R^{Crown} + \mathbf{S}_R^{Taper} + \mathbf{S}_A^{TCE\_0} + \mathbf{S}_A^{IMR\_0} \qquad \text{(Eq. 5)}$$

where

$\mathbf{S}_R$ ≜ Mill's overall mechanical deformation shape pattern at a particular operating point,

$\mathbf{S}_R^{NL}$ ≜ No-load transverse roll gap (typically based on bore geometry measurements with a nominal cluster),

$\mathbf{S}_R^{FSep}$ ≜ Separating force-loaded deflection (a function of the pass schedule),

$\mathbf{S}_R^{Crown}$ ≜ Mechanical crown influence (based on the transverse roll diameter profiles — typically idlers and work rolls),

$\mathbf{S}_R^{Taper}$ ≜ Mechanical taper influence (based on transverse roll diameter profiles — not associated with first IMR tapers),

$\mathbf{S}_A^{TCE\_0}$ ≜ TCE pre-set pattern influence and

$\mathbf{S}_A^{IMR\_0}$ ≜ Tapered first IMR rolls' pre-set pattern influence (this is a summation of both top and bottom influences)

One should be aware of the inclusion of the shape actuation pre-set terms ($\mathbf{S}_A$) terms for the TCEs and the first IMRs in Eq. 5.

The important thing to note is that, in all cases, the components of the physical shape/stress transverse waveform patterns (Eqs. 1a, and 1b) and Eq. 5 can be modeled and directly measured. This is the key to understanding and solving the problem.

Graphical Representations in Curvature Space — As shown in the first two articles in this series,[2,3] an important characteristic of the orthogonal polynomial basis is the ability to obtain a graphical representation of the situation from the curvature space perspective (i.e., "**$**"). This graphical representation provides indications of the directions to take for performance/quality improvement. Fig. 2 shows a pair of diagrams illustrating the components involved and how their vector summation define the force-loaded operating point.

To simplify the discussion and illustrations, it will be assumed that the first IMR pre-set and mechanical (ground in) taper within the roll cluster are both zero (i.e., $\$_A^{IMR\_0} = \$_R^{Taper} = 0$).

An examination of Fig. 2b shows the vector summation pathway provided by Eq. 3a and the transformed Eq. 5 (via Eq. 2). The nominal operating point is formed from the pass-scheduled force-loaded deflection, $\$_R^{FSep}$, and mechanical crown compensation, $\$_R^{Crown}$, applied to the initial conditions associated with the incoming strip, $\$_0$, and relaxed mill, $\$_R^{NL}$. As shown in Fig. 3a, the operating point can be extended to include the SACE (to form the *Offset* SACE), thereby indicating what the mill can do in this situation.

Taking the conditions of Fig. 3a, the shape actuation pre-sets are applied to the TCEs (vector addition to the nominal operating point and within the SACE). The result is depicted in Fig. 3b, which defines the operating point that is in effect for the given pass. It also provides an immediate indication of how much shape adjustment margin is available to the controller. In the case of Fig. 3b, the direction and amplitude of the TCE pre-setting places the operating point close to an SACE boundary, indicating the physical shape actuators are close to a limiting condition. This also shows the direction needed to travel from the shape actuated operating point, $\$_S$, to the flat shape target, $\$_T = 0$, which is a clear indication of the corrections/adjustments that need to be considered.

How to Proceed — Thus far, a series of relationships has been established (Eqs. 1a, 1b and 5) that provides a means of characterizing the mill/material interactions based on the waveform patterns of their influence on the rolled/exit strip shape. In all cases, the physical waveform characteristics of the mill deformation, shape actuator influences and

Figure 2

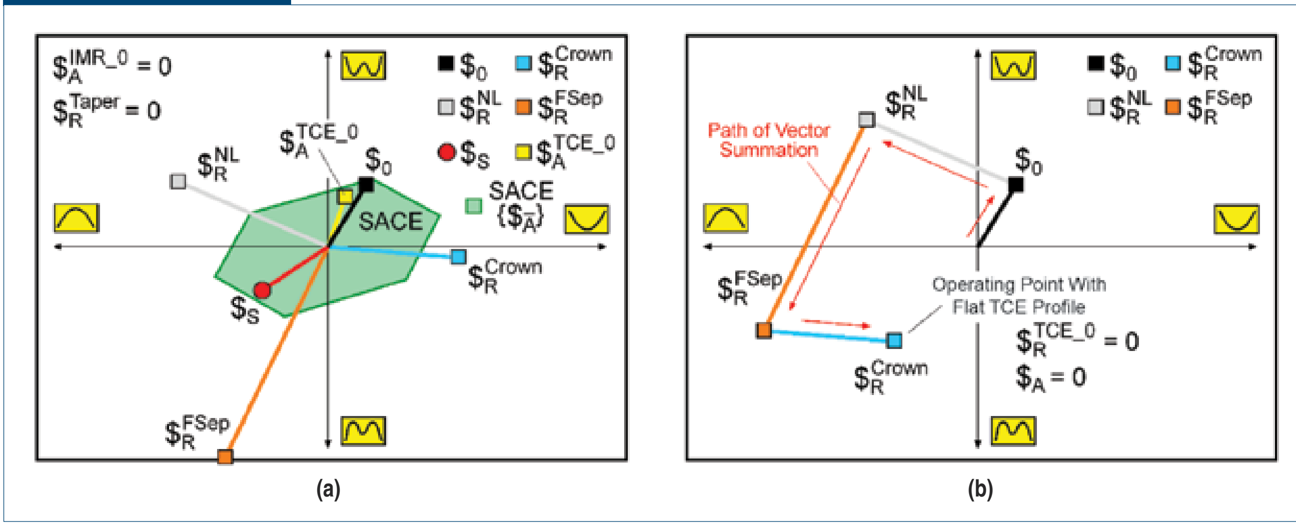

Curvature space diagrams: plots of the individual components (a), and plot of the vector summation forming the nominal, force-loaded operating point (b).

rolled shape (i.e., "**S**") can be directly measured. Using the orthogonal polynomial transform, $\tilde{\mathbf{P}}$, in Eq. 2, it is possible to seamlessly switch between the physical dimensions and the curvature framework (via simple matrix algebra). In the spatial curvature framework (i.e., "**\$**"), the behavior and characteristics of the mill/material interaction and resulting rolled/exit shape can be graphically depicted and visually assessed. In this graphical representation, the directions needed to be taken to improve the situation and correct the problem can be assessed. These corrective adjustments can then be transformed back into the physical space, ready for implementation.

In general, this can be distilled down to a five-step procedure:

1. Take measurements and collect data in the physical world.
2. Transform them to their curvature framework representations.
3. Examine and evaluate the situation in the curvature framework.
4. Determine a solution in the curvature framework.

Figure 3

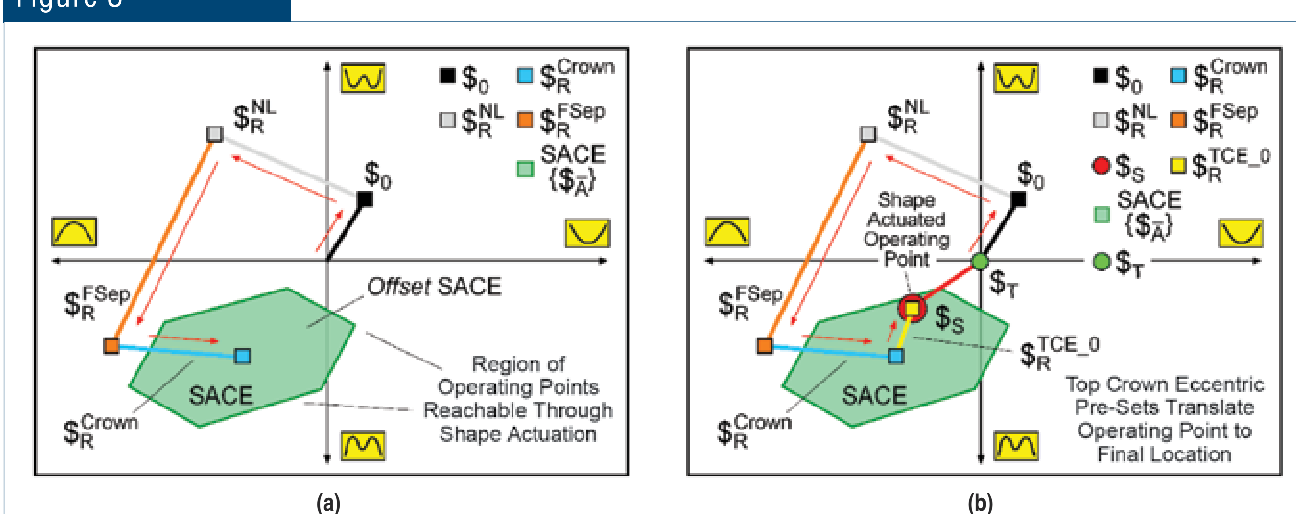

Curvature space diagrams: plots of the individual components (a), and plot of the vector summation forming the nominal, force-loaded operating point (b).

5. Transform the solution back to physical world adjustments/corrections (ready for implementation).

Characteristics of the Force-Loaded Mill and Its Setup

Measuring the Uncompensated, No-Load Mill Geometry

— A first course of action is to determine the no-load transverse roll gap formed from housing bore geometry/orientation measurements and a nominal (uncompensated) roll cluster arrangement. This determination provides important insight into the fundamental geometry of the roll cluster and forms the initial condition from which the force-loading deflections will evolve. Fig. 4a provides a diagram showing the optically measured bore geometries and orientations of the ZR23-26 housing.

In this case, the housing's bore surfaces were in good condition and the general nature of the bore orientations followed a consistent machining tool wear compensation pattern (nominally sloped downward to the rear and kicked to the left) associated with classical manufacturing practices. However, some bore distortions are observable; most notably, the tapering/lifting actions of the F and G bores toward the front, the splaying/lifting action of the B and C bores toward the front, and the concave crowning of the D and H bores. This not uncommon in housings that were machined using unsupported boring bars.

Although not an issue in this situation, older housings may be subject to imprint and scoring/gouging damage along the bore surfaces (due to the mishandling of the backing shafts during insertion). Imprint damage is associated with small, metallic particles (scraps) being caught in between the bore and saddle base surfaces. Gouging damage is due to the physical scraping and displacement of bore surface material. In both cases, there is typically an indented region with an adjacent prominence (or pad) of relocated bore surface material.[7] This pad of displaced material acts as a localized pedestal that lifts the saddle base from the bore surface, leading to misalignment and a possible source of shape distortions in the rolled/exit strip. This type of prominence/pad must be carefully scraped to achieve a smooth bore surface and assure proper seating of the saddle base and alignment.

Using a nominal roll cluster (i.e., nominal roll diameters with flat profiles: $\mathbf{S}_R^{Crown} = \mathbf{S}_R^{Taper} = 0$) with the TCEs set to "flat" nominal (i.e., $\mathbf{S}_A^{TCR-PreSet} = 0$) and the taper knees of the first IMR rolls moved the planned strip edge (i.e., maximum effective flat with $\mathbf{S}_A^{IMR-PreSet} = 0$), the no-load transverse roll gap was

Figure 4

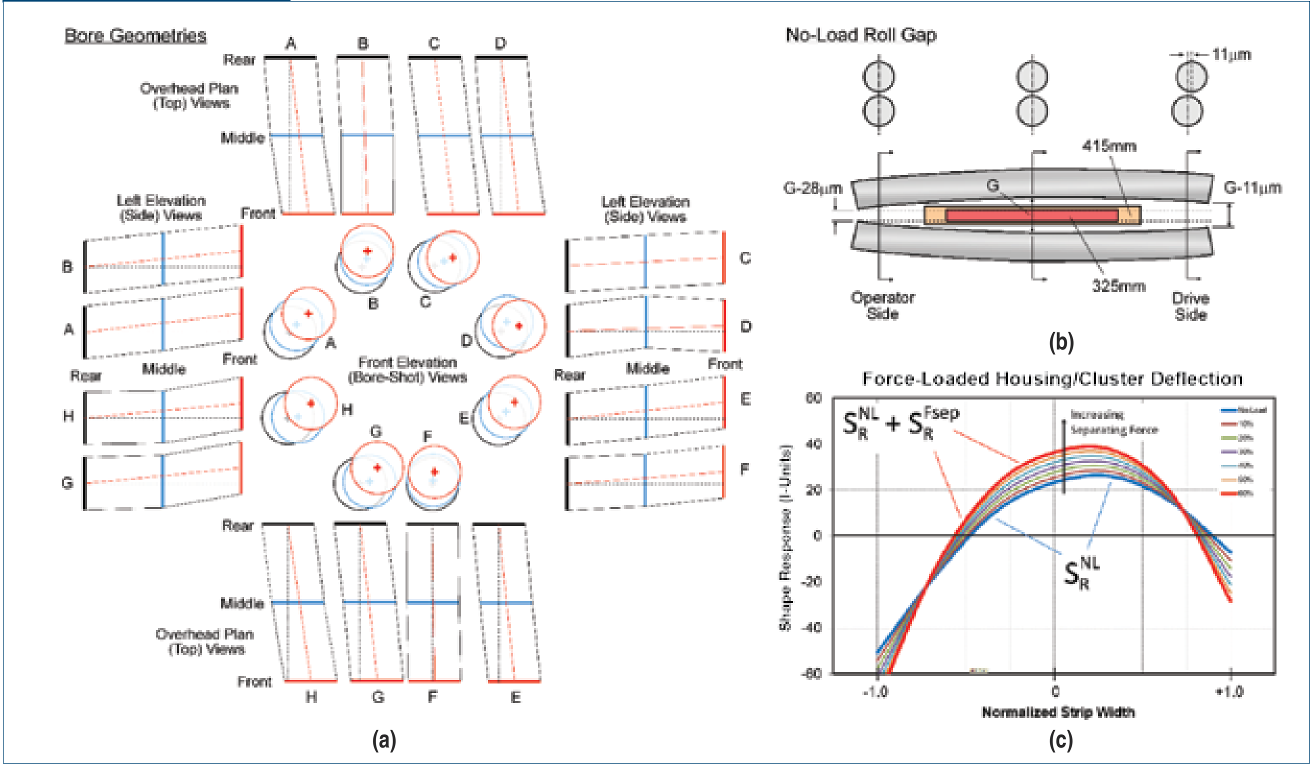

Diagram showing: housing's bore geometries and orientations (a); no-load roll gap geometry (b); no-load roll shape pattern and associated separating force progression (c).

determined and is shown in Fig. 4b. The gap shows a very strong convex crowning with a substantial tilt/skew to the operator side, illustrated in the shape pattern $\mathbf{S}_R^{NL}$, shown in Fig. 4c.

This is a difficult situation because the no-load conditions require a substantial crowning addition (before force-loaded deflection compensation is even considered) and the TCE shape actuation would be expected to address the tilt/skew component.

Measuring the Force-Loaded Deflection and Shape Actuation Influences — The force-loaded deflection and influences of the shape actuators were measured using a combination of static and dynamic evaluations:

- **Static Evaluation —** The static method involved imprinting the loaded roll gap onto precisely inserted samples of mid-alloy brass and low-carbon steels (as done in Reference 8). The sample widths (425 mm) corresponded to nominally full-width edge-cut strip. Fig. 5 shows several of these samples. The applied forces ranged from 10 to 60% of the mill's rating. The imprinted roll gap profiles were measured in 10-mm intervals (with respect to the operator side) to render the indications of the mill's transverse deflection.
- **Dynamic Evaluation —** The dynamic tests were conducted while rolling, and involved applying on-line perturbations in the shape actuation settings, at a progression of separating force settings, and measuring the differential shape patterns that were observed by the shapemeter (as done in Reference 6). Evaluation of these patterns/waveforms determines the individual shape actuator's spatial influence function.[2]

The static and dynamic test results showed good correlation and provided reasonably accurate depictions of the force-loaded deflection behavior. Fig. 4c shows the shape waveform pattern of the nominal mill deflections (shape actuation set to nominal) over the tested separating force range ($\mathbf{S}_R^{NL} + \mathbf{S}_R^{FSep}$). The separating force loading component, $\mathbf{S}_R^{FSep}$, had a strong, symmetrical convex deformation.

Due to the narrow geometry of the strip, the TCE shape actuation response characteristics were dominantly first and second order, indicating a low dexterity and very limited shape correction capability.

Figure 5

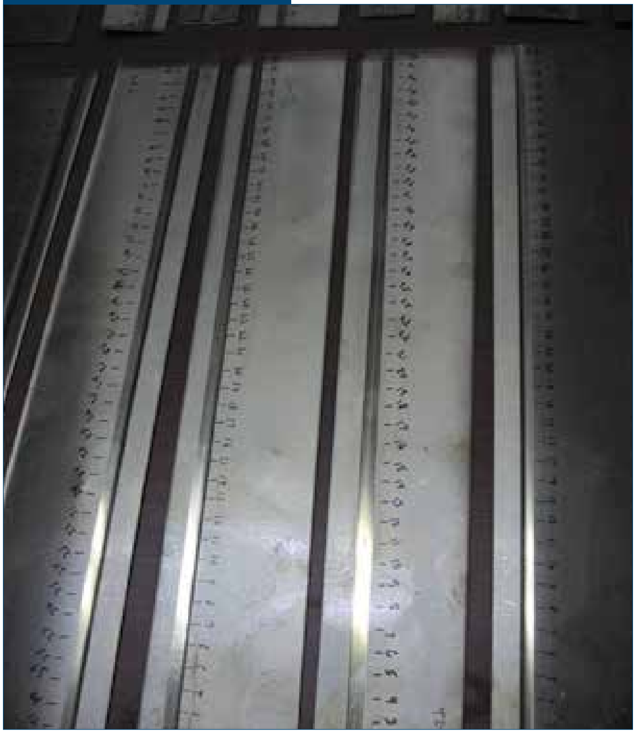

Roll gap imprint testing samples.

Table 1

Typical Roll Cluster Setup

Rolls	Crown Physical (µm)	Crown Roll bite (µm)	Tapers Slope (µm)	Tapers Length (µm)
Work rolls (total)	0–100	0–120	—	
First IMRs	—		—	
Step 1	—		1.2	—
Step 2			0.4	30
Second IMRs	—		—	
Top idler	Flat	0		
Bottom idler	200	90	—	
Drive rolls	Flat	0		

Influence of Mechanical Crown and TCE/IMR Pre-Sets — The roll cluster's setup is based on the mechanical crowns and tapers applied to the rolls. Table 1 lists the typical roll arrangements. The "physical" crown indication is associated with the rolls' transverse diameter profile, while the "roll bite" indication is the effective crown as realized at the roll bite[7] in the presence of the inter-roll contact/transmission attenuation. The mechanical crown influence function, $\mathbf{S}_R^{Crown}$, shown as the red curve in Fig. 6a, amounts to approximately 170 mm of effective crown in the roll bite. Similar mills rolling narrow material often employ 200–300 mm of effective total crown[7,9,10] depending on typical separating force levels. This arrangement suggested a lack of mechanical crown in the cluster. No overall tapering is applied, $\mathbf{S}_R^{Taper} = 0$, for all cases.

As shown in Fig. 6b, the TCE pre-set arrangement, $\mathbf{S}_A^{TCE\text{-}0}$, is highly crowned, with a clear offset

Figure 6

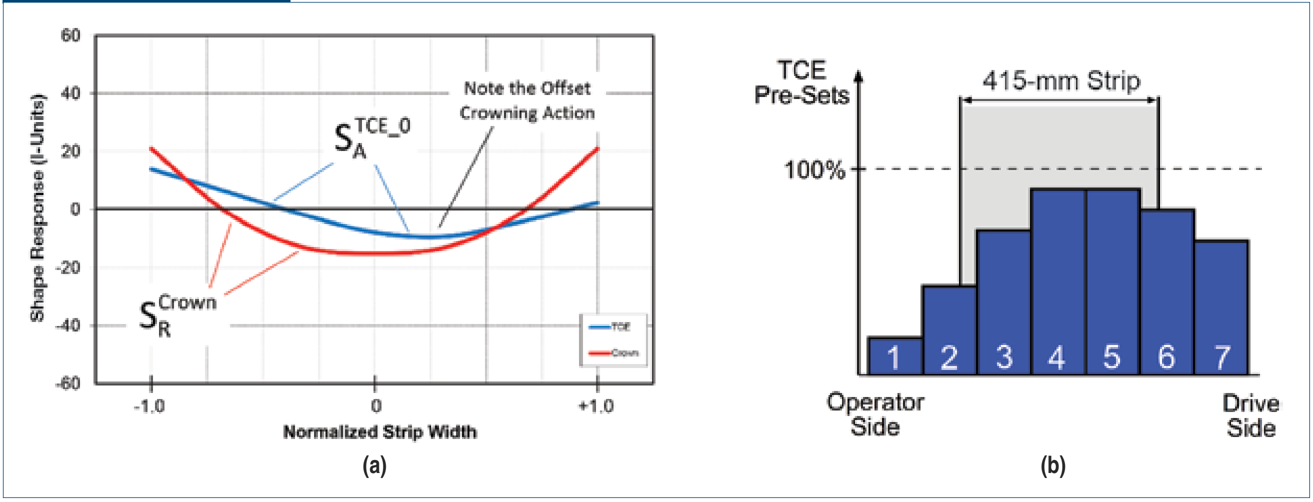

Diagrams of TCE pre-setting pattern (a) and shape influences of mechanical crowning and TCE pre-sets (b).

to the drive side. These settings were determined by the mill operators and had become a standard operating practice. It is interesting to note that the TCE crowning influence (see Fig. 6a) amounts to approximately 70 mm of added crown in the overall cluster, thereby making the total effective crown on the order of 240 mm, which complies with suggested amplitudes.[1,9,10] Essentially, the TCE pre-set crowning provides the added static crown lacking in the cluster's mechanical crowning (as noted above); however, this resulted in a significant restriction in the available TCE control range (i.e., reduced margins). The TCE crown offset (Figs. 6a and 6b) appears to properly coincide with the offsetting nature of the cluster deflection, associated with the housing bore geometry, shown in Fig. 4.

Table 1 lists the two-step tapering method for the first IMRs. The Step 1 taper length is a function of the strip width and stroke length of the actuating hydraulic cylinder, and, therefore, is not listed. The Step 2 taper is provided as a means of smoothing the taper knee transition, to avoid inducing quarter-buckle-like distortions. The first IMR pre-set locations were typically 25–40 mm inboard of the respective strip edges, with their shape-targeted responsibilities having a marginally flat to slightly over-rolled (pie-crust edge crack protection) conditions. As noted in Part 1 of this study,[1] the defect primarily occurs when rolling wedge strip, with the thicker edge to the operator side. Also, a slight bias in the first IMR symmetry was generally noted, with the operator-side taper depth operating in the 30–35 mm vicinity, while the drive side settled in the 20–25 mm region. As shown in Fig. 7, this off-centered taper geometry (shifted effective flat) causes an asymmetric influence on the rolled shape and correlates with the roll gap geometry noted

Figure 7

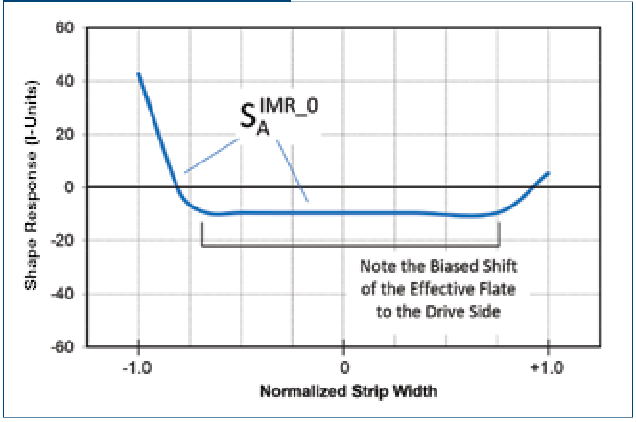

Spatial influence function of the composite top and bottom first IMRs.

in Fig. 4. The sustained negative value in the effective flat region is associated with the necessary condition of preserving a zero mean in the shape response. It is important to note that the depth of the operator-side taper (although deeper than the drive side) was far shorter than the location of the defect. Careful testing[1] showed that the root cause of the defect was not attributable to the first IMR tapering conventions.

Work Roll Thermal Crown and Wears — Direct measurements of the work roll's thermal crown growth and wear characteristics were performed using a precision, laser-based roll diameter profiling system, with 1.0 µm resolution. The diameter profiles of recently ground and prepared work rolls at room temperature were measured to establish initial conditions. These rolls were installed in the mill and rolling operations were performed. As the rolls were changed (at rolling temperatures), their temperatures and diameter profiles were immediately taken to obtain a measure of the combined thermal crown growth and roll wear. Days later, and now at room temperature, diameter profiles were again taken to determine the wear. This measured wear profile was then subtracted from the higher, rolling temperature profile to determine the thermal growth characteristics.

Selected 7- and 9-pass scenarios were used in the rolling trials, with a work roll change prior to rolling the last pass. Various combinations of crowned and flat work rolls were used. The 6- and 8-pass work rolls and the final pass work rolls were measured to determine if the diameter profile distortions in the early passes were inducing the problem or if only the last pass rolls were the source. In general, all work rolls experienced a 25–30°C temperature rise at the roll centerline with only a minor drop-off at the edges. A consistent, relatively smooth thermal crown was noted in the strip contact region, on all work rolls ranging from 12–16 µm, regardless of mechanical crown or duration in the mill. Away from the strip contact area and toward the edge there was a moderately sharper drop-off. The wear pattern appeared as a relatively flat, trough-like depression aligned with the nominal strip contact region, ranging ~4–6 µm deep.

Combined, these consistent variations in the work roll diameter profile were highly symmetric and accounted for approximately 10% of the mechanical crown on the work roll (alone). These effects did not correlate with the defect pattern, allowing the work roll thermal crown and wear characteristics to be eliminated from consideration.

Dissecting the Defect Formation

As shown in Fig. 8a, this is a very curious and confounding defect (and please be aware of the rescaling of the plotted data). Although similar to a quarter-buckle, the operator-side asymmetry does not align itself with expectations, and classical approaches to resolving this flatness distortion had little impact. For this case, the localized buckling threshold is approximately 16 I-units in compression (negative values), and the region of manifest flatness distortion is indicated as shape content falling below the threshold.

The above findings suggest a clear tapering/skewing and concave crowning associated with the housing, when projected to the roll bite, in both a relaxed and force-loaded condition. This suggests a need for a moderately high level of mechanical crown in the overall roll cluster (larger than would be expected for this class of mill). Coupling this skewing/crowning issue with the operator-side wedge strip profile only compounds the difficulties. The TCE pre-set pattern appears to address these crown and skewing deficiencies; however, these settings are close to the step-limits constraints,[2,3,7] leaving little dynamic margin to work with. While the TCE pre-set is in the proper corrective direction, there is a sense that there is insufficient amplitude to complete the job.

The drive-side shifted bias in the first IMR presetting also correlates with the closed operator-side tendency of the housing (i.e., the taper depth of the top first IMR induces a tightening of the loose edge shape formed by the housing distortion); however, at ~30 mm, the taper knee is not deep enough to form the defect. Further, it's important to recall that trial modifications of the first IMR taper geometry did not have a significant impact on the defect.

Figure 8

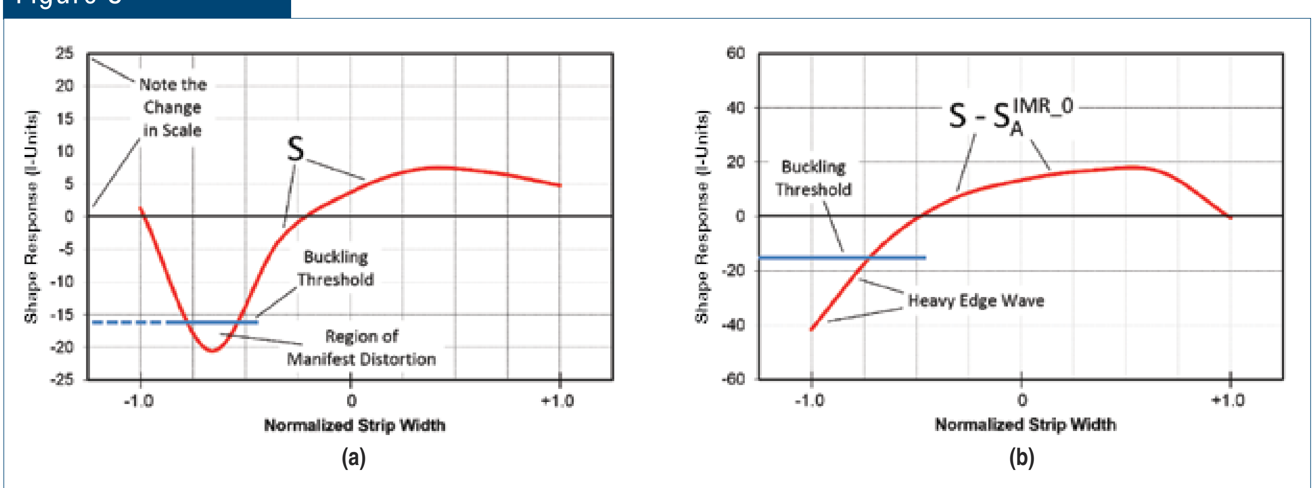

Diagrams illustrating the defect shape: measured shape of the rolled/exit strip (a) and remnant defect shape (b).

Influence of the First IMRs — As noted above and in Part 1 of this case study, modification and testing of variation in the taper characteristics of the first IMRs had little effect on the defect's resolution. To gain greater analytic insight into the underlying cause of the defect, the influence function of the first IMRs was removed from the defect's measured shape. The resulting waveform pattern is shown in Fig. 8b.

The most immediate result in Fig. 8b is the removal of the sharp, narrow defect depression. However, the remnant is a very strong operator-side edge wave characteristic (that is basically unrollable). The important point here is that the top first IMR (operator-side taper) is responsible for maintaining a narrow region of the operator-side strip edge in a reasonably tight state. In doing this, the first IMR's taper knee must be drawn into the interior of the strip body to generate sufficient relief of the heavy over-rolling of the operator's side region. Therefore, the narrow first IMR action lifts the deepening operator's side region of Fig. 8b, to the extent show in the Fig. 8a, forming the ascending operator-side slope of the defect depression.

However, although the action of the first IMR may appear to be a direct contributing component in the defect, it is not the root of the defect formation; it is purely a coupled reaction of a shape actuator focused on its narrowly defined responsibility, in the presence of a heavily over-rolled edge condition.

Discussion: Root Cause of the Defect — The intent of this case study is to illustrate how to use the developed analytic method[2–5] to immediately identify the root cause of the defect formation and to provide clear directions for resolving the problem. Before pursuing the analytic method, it is important to expose the underlying mechanism of the defect formation to provide insight into how the method works.

The remnant waveform of Fig. 8b is the result of the removal of the first IMR influence and reveals that the combined roll cluster's mechanical crown, and the added effective crown of the TCE pre-set does not have sufficient compensation to overcome the force-loaded deflection of the roll cluster at the pass-scheduled operating point, in the presence of the housing's bore deformations.

The bottom line is there is not enough total crown in the mill and not enough remaining tilting/skewing capacity in the step-limited TCE control range. When combined with the activities of the properly applied top first IMR, the experienced defect forms.

Fig. 9 shows this lack of crown/tilt compensation through a comparison of the force-loaded deflection and the mechanical crown/TCE compensation (see Fig. 6a). The defect is formed by the accelerating separation of the operator-side deflection of the roll cluster/housing (primarily associated with the bore geometries), which exceeds the compensation "steepness" of the mechanical crowning and TCE pre-set.

Figure 9

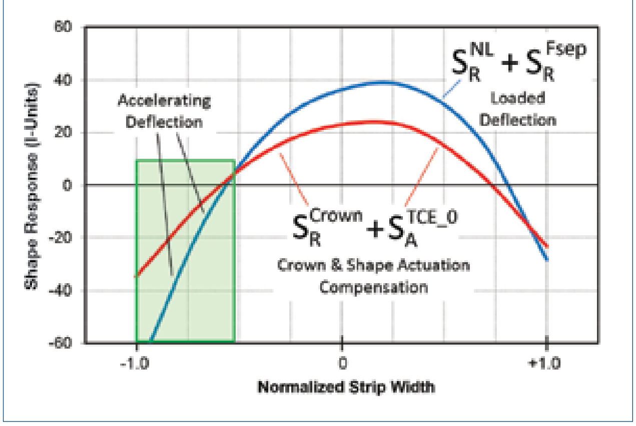

Root cause of the defect, deformation vs. compensation.

From a defect source/resolution-finding perspective, working with spatial waveforms provides an understanding of the defect formation, but it's not always immediately clear and there's no way to ascertain the impact of the shape actuation limitations. Alternatively, working within the spatial curvature framework provides immediate indications and directions for resolving the problem.

Decomposing the Components — To better examine the underlying nature of the defect, the individual components are decomposed into their fundamental spatial curvatures using the orthogonal polynomial transformation of Eq. 2.[2] It is important to recall that all of the individual component characteristics were measured (see the section entitled "Characteristics of the Force-Loaded Mill and Its Setup"). Due to the asymmetric characteristics of the defect, it is necessary to include the odd-order curvatures. Fig. 10 provides vector plots of the components and adheres to Fig. 8b's first IMR exclusion.

Determining the Operating Point — Using the vector summations of the section entitled "Understanding the Involved Components" and their associated graphical representation of Figs. 2 and 3, the *Offset* SACE is formed/located for the force-loaded conditions, and with the application of the TCE pre-set, the operating point is defined. Fig. 11 provides curvature space diagrams showing the odd- and even-order operating point constructions, along with indications of the directions of migrations for change to the roll cluster's mechanical crown and taper/skew.

The "red dot" designated operating points (and vectors) shown in Fig. 11 define the curvature components that form the remnant spatial waveform of Fig. 8b. The positive first-order curvature in Fig. 11a

Figure 10

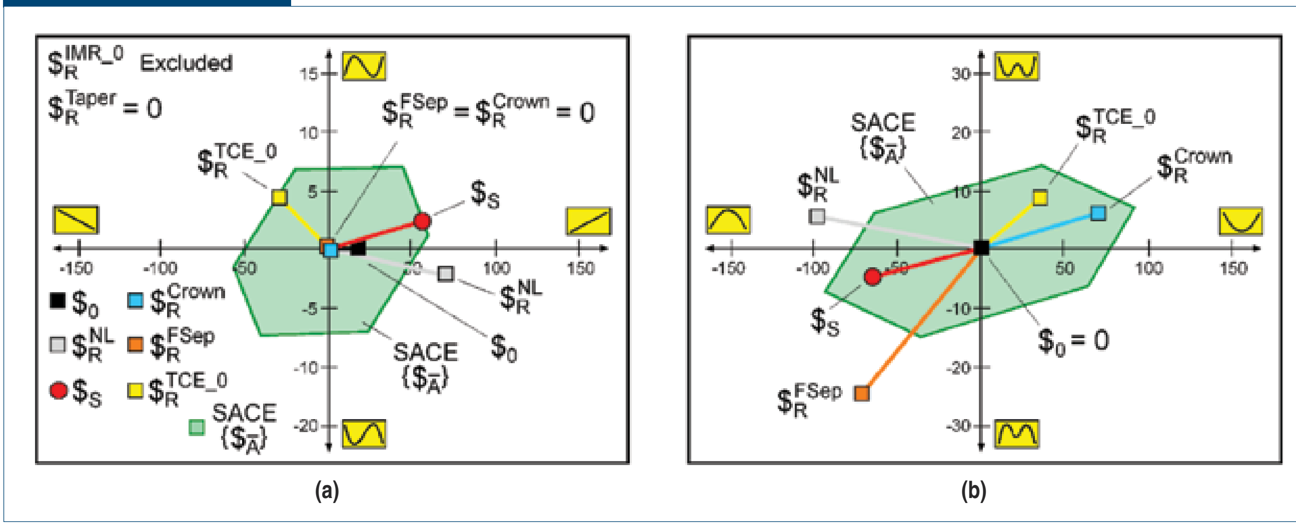

Curvature space diagrams of the individual components: odd-order curvatures (a) and even-order curvatures (b).

and the negative second-order curvature in Fig. 11b are obvious results, given the general form of Fig. 8b. However, the presence of mild positive third-order and negative fourth-orders are not intuitive outcomes, but are associated with producing the drive-side flat and sharper curvature.

Discussion: Immediate Identification of the Defect — In the simplest case, eliminating the shape defect is only of interest, and therefore a flat shape target ($\$_T = 0$ at the origin of both odd/even curvature spaces) will be considered. An examination of the curvature space diagrams of Fig. 11 provide immediate insight into the formation of the defect and the situation at hand. In both cases, the *Offset* SACEs do not overcontain the origin and the operating points lie near the extents of the *Offset* SACEs.

In the odd-order curvature space of Fig. 11a, there is a clear need for additional taper (i.e., the *Offset* SACE is too far to the positive/right side). In the even-order curvature space of Fig. 11b, there is a clear need for additional positive crown (i.e., the *Offset* SACE is too far to the negative/left side). Applying sufficient taper and crown will translate the *Offset* SACEs toward the origin and resolve the shape defect problem.

The graphical depictions and suggested courses of action indicated in Fig. 11 are in agreement with the comments in the section entitled "Discussion:

Figure 11

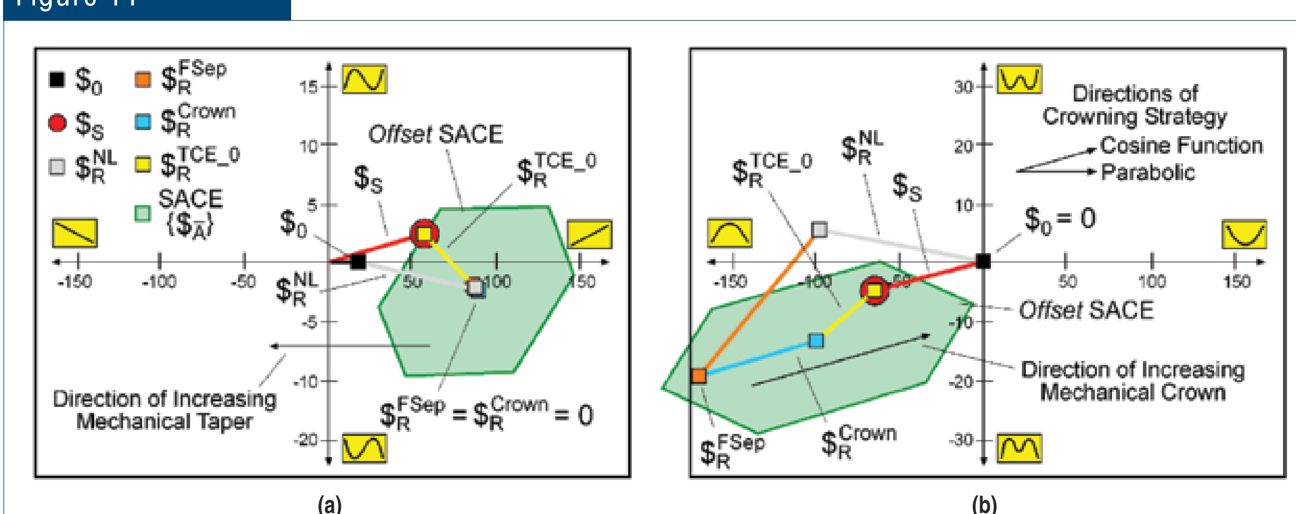

Curvature space diagrams showing the vector summation forming the nominal, force-loaded operating point associated with the defect: odd-order curvatures (a) and even-order curvatures (b).

Root Cause of the Defect." Further, these graphical representations show how and why the defect is being formed.

1. In Fig. 11a, the asymmetric distortion in the no-load transverse roll gap, $\mathbf{S}_R^{NL}$, is the lone reason the odd-order *Offset* SACE is translated from the origin. The extent of this translation is beyond the restoring capabilities of the TCE shape actuation.
2. In Fig. 11b, the no-load transverse roll gap induces a convex crowning action that, when combined with the nature force-loaded deflection, $\mathbf{S}_R^{FSep}$, translates the even-order *Offset* SACE from the origin, exceeding the range of TCE shape actuation.
3. In Fig. 11b, the mechanical crown in the roll cluster is not sufficient to overcome the combined effects of the housing bore distortions and the force-loaded deflection.

Resolving the Defect Formation

Beyond indicating the defect formation mechanisms, the curvature space diagrams of Fig. 11 provide direct insight into what is needed to resolve the problem. The objective is moving the operating point toward the origin of the odd and even curvature spaces. As shown in Fig. 12, this amounts to increasing positive/convex crown and transverse taper in the roll cluster.

Ideally, the *Offset* SACEs should be centered at the origin, thereby maximizing the available control range of the TCE shape actuators. Unfortunately, this may not be completely realizable due to limitations in the profiling capabilities of the existing roll grinding equipment (i.e., be limited to simple parabolic or cosine functions), along with a need to consider thermal crown growth effects.

In considering these corrective actions, one also needs to take into account where (within the roll cluster) the required levels of crown and taper adjustments can be implemented and sustained in the presence of a desire to make minor adjustments to the effective crown through work roll diameter profiles. Taking this into account, the following approach was undertaken:

1. The asymmetries in the housing bore geometry (and associated no-load roll gap of Fig. 4b) are addressed through a full-width, monotonic tapering of the top second IMR idler roll. To accommodate the transmission attenuation (to the roll gap) experienced by the second IMR idlers, the 17 µm tilt/skew requires approximately 40 µm of taper across the roll face (a taper slope of 0.06 µm/mm).
2. The increase in the cluster's total crown is addressed by crowning the bottom second IMR idler roll. It was desired to reduce the work roll crown range to 0–60 µm and to increase the cluster's total mechanical crown to have an effective crown of approximately 240 µm. This required 400 µm of mechanical crown on the bottom second IMR idler roll. Although a larger mechanical crown could be provided, it was desired to induce a very slight crown in the pre-setting of the TCEs.

The rationale for using this approach is that the top second IMR idler is mechanically suspended and

Figure 12

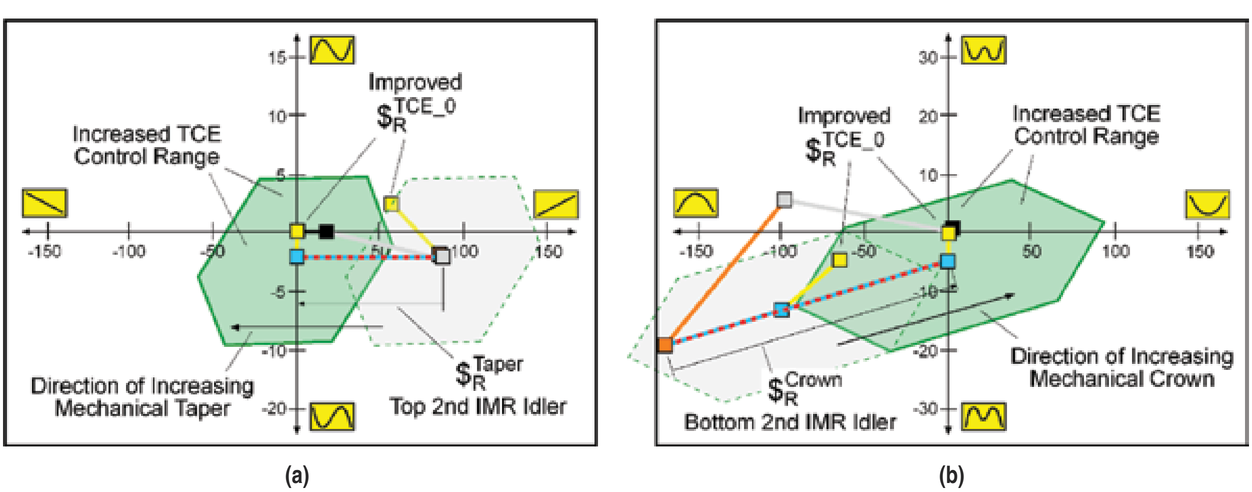

Curvature space diagrams showing the actions needed to correct the shape defect: odd-order curvatures (a) and even-order curvatures (b).

Figure 13

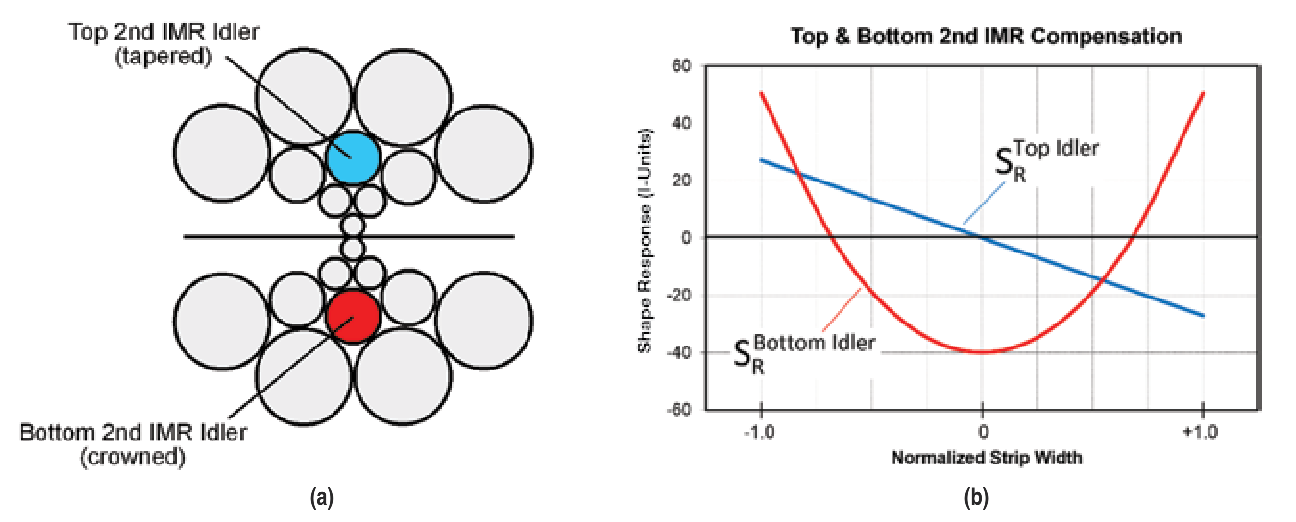

The corrective adjustments made to the roll cluster mechanical crown/taper: cross-section of the roll cluster with color-coded second IMR idler rolls (a), and shape influences of the top idler tapering and the bottom idler crowning (b).

not easy to change, so the taper correction is applied there. The bottom second IMR idler is gravitationally held and easier to access/change, allowing the corrective crowning to be applied along with other crowning components to support strip width changes. Fig. 13 provides an overview of these roll cluster profile adjustments, while Table 2 lists the corrective adjustments.

Installing these changes in the roll cluster setup provided an immediate resolution of the defect. No indications of the defect were noted by visual assessments of the strip or in the shape measurements. Even with the high level of total cluster crown, there was still a need to apply some degree of crowning through TCE pre-setting. Some changes in the first IMR presetting locations were noted and these adjustments coincided with the correction of the asymmetries in the housing bore geometries.

Fig. 14a provides diagrams showing the compensating effect of the second IMR idler roll crowning and tapering. It is important to note how the operator-side separation (of Fig. 9) has been strongly suppressed; however, some degree of general crowning separation is still present (to be addressed by the TCE pre-setting of Fig. 14b).

The approach taken here has been to address the symmetric and asymmetric aspects of the mill housing distortions and material profile by modifying the roll cluster's mechanical crown and taper profiles.

In its entirety, this strategy is not the only way to handle the problem. The tapering issues must be accommodated by mechanical profile modification; however, the crowning aspects can also be slightly altered by adjusting the pass-scheduled earlier pass reductions to permit lighter reductions in the last couple of passes. This has the effect of reducing the separating force-loaded deflection of the roll cluster on the important last pass, thereby requiring less compensating mechanical crown. This approach can provide a wider range of applicability for the bottom second IMR idler roll's chosen crown (i.e., one can roll and larger range of wider material without changing the roll's crown profile), which may be more palatable to the overall production mix to be rolled on this mill.

Table 2

Corrected Roll Cluster Setup

Rolls	Crown		Tapers	
	Physical (μm)	Roll bite (μm)	Slope (μm)	Length (μm)
Work rolls (total)	0–50	0–60	—	
First IMRs	—		—	
Step 1	—		1.2	—
Step 2			0.4	30
Second IMRs	—		—	
Top idler	—		0.06	650
Bottom idler	400	180	—	
Drive rolls	Flat	0		

Conclusion

This article concludes a two-part case study and brings to a close this six-part series by showing one

Figure 14

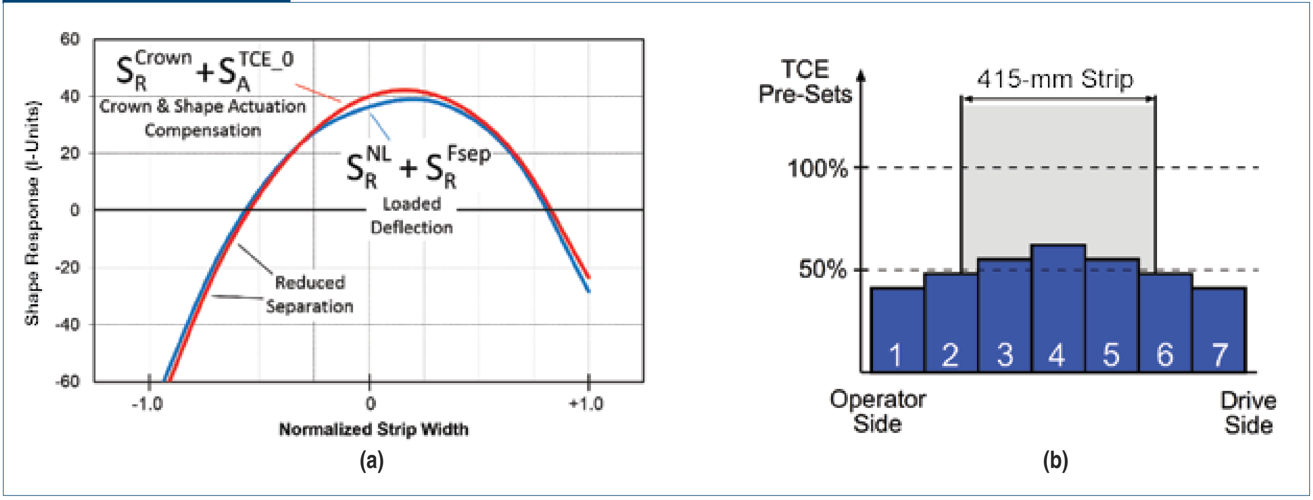

Diagrams showing: how the corrections to the roll cluster's total crown reduced the defect-inducing operator-side separation (a), and new amplitudes of the TCE pre-sets (b).

way to apply the developed systematic method of using an orthogonal polynomial-based transformation to expose the curvature components of the contributing spatial waveforms of the mill, material and shape actuation. The problem that has been examined is an odd and curious asymmetric shape defect occurring on narrow-wedge profiled strip rolled on a wider mill. Initial attempts to resolve the defect did not respond to classical methods. Applying this analytic method in concert with measurements of the housing bores, force-loaded roll bite conditions and shape actuation influence functions immediately indicated the primary source of the problem, which turned out to be associated with geometric distortions in the housing bores in combination with a general lack of total crown in the roll cluster. The analytic method also provided directions of resolution that suggested a mechanical crowning/tapering solution. Rolling trials with the modified roll cluster achieved immediate improvements and no presence of the defect was noted in visual assessments and on-line shape measurements.

Overall this new analytic method has been applied to variety of situations, including coordinated pass scheduling, shape target progression selection, roll cluster/stack profile selection and on-line shape control systems. Although much of this series has been dedicated to the complexities of 20-high cluster/Sendzimir mills, it has also been successfully applied to vertical stack configurations (i.e., 4-highs and 6-highs). Current plans are to continue with the application of this method to other mill types and rolling applications, along with helping mill operators and process designers to better understand complex and confusing shape-related problems that they may encounter or be experiencing.

References

1. Zipf, M.E., "Resolving Complex Shape Distortions on Narrow, Thin-Gauge Strip Having an Asymmetric Transverse Thickness Profile — Case Study: Part 2 — Defining the Problem," *Iron & Steel Technology,* Vol. 13, No. 5, 2016, pp. 86–96.
2. Zipf, M.E., "Method for the Determination of Shape Actuator Capabilities Envelopes in 20-High Cluster Mills," *Iron & Steel Technology,* Vol. 9, No. 12, 2012, pp. 77–89.
3. Zipf, M.E., "Multivariable Directions in the Improvement of Shape Actuator Performance," *Iron & Steel Technology,* Vol. 10, No. 2, 2013, pp. 106–123.
4. Zipf, M.E., "Multivariable Shape Actuation Capabilities Envelopes of Vertical-Stack Mills," *Iron & Steel Technology,* Vol. 11, No. 2, 2014, pp. 46–61.
5. Zipf, M.E., "A Unifying Spatial Curvature Framework for Coordinated Pass Scheduling, Shape Targeting and Mill Setup," *Iron & Steel Technology,* Vol. 11, No. 12, 2014, pp. 86–97.
6. Zipf, M.E.; Godwin, C.K.; and Wisti, D.R., "Comparative Studies of Sendzimir Mill Shape Control Responses," *AISTech 2008 Conference Proceedings,* Vol. II, 2008, pp. 389–399.
7. Duprez, J.L., and Turley, J.W., *The Sendzimir Manual,* T. Sendzimir, Inc./Jean-Louis Duprez Publications, Waterbury, Conn., USA, 2000.
8. Turley, J.W.; Pollastrelli, A.; and Brecy, M., "Control of Quarter Buckle on Sendzimir 20-H Mills," *Proceedings of Iron and Steel Engineers,* Pittsburgh, Pa., USA, 1999.
9. Duprez, J.L., personal conversations and discussions, 2004–2012.
10. Richcreek, D.M., personal conversations and discussions, 2004–2013.

✦

To nominate this paper for the AIST Hunt-Kelly Outstanding Paper Award, visit AIST.org/huntkelly.

This paper was presented at AISTech 2015 — The Iron & Steel Technology Conference and Exposition, Cleveland, Ohio, USA, and published in the Conference Proceedings.